Band-gap engineering in TiO_2-based ternary oxides

J. A. McLeod*
Department of Physics and Engineering Physics, University of Saskatchewan, 116 Science Place, Saskatoon, Saskatchewan, Canada S7N 5E2

R. J. Green
Department of Physics and Engineering Physics, University of Saskatchewan, 116 Science Place, Saskatoon, Saskatchewan, Canada S7N 5E2

E. Z. Kurmaev
Institute of Metal Physics, Russian Academy of Sciences–Ural Division, 620990 Yekaterinburg, Russia

N. Kumada
Department of Research Interdisciplinary, Graduate School of Medicine and Engineering, University of Yamanashi, Miyamae-Cho 7, Kofu 400-8511, Japan

A. A. Belik
International Center for Materials Nanoarchitectonics (WPI-MANA), National Institute for Materials Science (NIMS), 1-1 Namiki, Tsukuba, Ibaraki 305-0044, Japan

A. Moewes
Department of Physics and Engineering Physics, University of Saskatchewan, 116 Science Place, Saskatoon, Saskatchewan, Canada S7N 5E2
(Received 29 June 2011; revised manuscript received 17 February 2012; published 4 May 2012)

The electronic structure of several ternary oxides (Sn_2TiO_4, $PbTiO_3$, $Bi_2Ti_4O_{11}$, and $Bi_4Ti_3O_{12}$) based on binary lone-pair oxides (SnO, PbO, and Bi_2O_3) and a d^0 oxide (TiO_2) is investigated using soft x-ray spectroscopy and electronic-structure calculations. We find that the valence band of these ternary oxides is bounded by bonding (at the bottom of the valence band) and antibonding (at the top of the valence band) O $2p$ lone-pair ns (Sn $5s$, Pb $6s$, Bi $6s$) hybridized states, while the conduction band is dominated by unoccupied Ti $3d$ states. The existence of these two features is found to be independent of crystal structure or stoichiometry. The calculated hybridization in the bonding O $2p$ lone-pair ns states is in reasonable agreement with the relative intensity of this feature in the measured x-ray emission spectra. The dominant influence on the conduction and the valence bands in the ternary oxides is due to different aspects of the electronic structure in the parent binary oxides, and we consequently find that the band gap of the ternary oxide is found to be a stoichiometric-weighed addition of the band gaps of the parent oxides.

DOI: 10.1103/PhysRevB.85.195201 PACS number(s): 71.20.Gj, 71.15.Mb

I. INTRODUCTION

The search for more efficient host materials for solar-driven hydrogen production has brought metal oxides (such as TiO_2, ZnO, and Fe_2O_3) into the light of renewed scientific attention in the last few years.[1] Of these binary metal oxides, TiO_2 is one of the most promising photoanode materials for water splitting using solar radiation because of its suitable band structure, including a band gap straddling the reduction and oxidation potential of water, and low cost and high-corrosion resistance in a wide variety of aqueous electrolytes.[2] However, the band gap of TiO_2 is too large (3.03 eV for rutile[3] and 3.2 eV for anatase[4]) to absorb a significant part of the visible spectrum. Only UV radiation, which is about 4%–5% of the solar spectrum, can drive photoconversion in TiO_2.[5] To achieve an acceptable hydrogen conversion efficiency (i.e., 15% or more), the band gap must be reduced below 2.2 eV.[6] Therefore, the band-gap reduction of TiO_2 is a key requirement for effective utilization of solar radiation. One way of reducing the band gap for the next generation of TiO_2-based photocatalysts is to combine multiple anions or cations to form ternary (or even more complex) oxides. Of all the possible ways of forming ternary oxides, four areas of research are of immediate promise for band-gap reduction:

(1) Doping TiO_2 by replacing oxygen atoms with anions having higher $2p$ orbital energy (such as B, C, and N), creating bands[7,8] or defect states within the nominal band gap.[9–12]

(2) Replacing Ti (d^0) with $3d^n$ and $4d^n$ cations (such as V, Cr, Nb, or Mo) introducing d character to the valence band.[13,14]

(3) Replacing Ti atoms with with $3d^{10}$ cations (such as Zn, Cd, or Ga) inducing $3d^{10}$–O $2p$ repulsion.[15]

(4) Replacing Ti atoms with heavy-metal ns^2 cations (such as Sn, Sb, Pb, or Bi) because of participation of $5s$ or $6s$ lone pairs in chemical bonding with O $2p$ states.[16,17]

Of course, a combination of these approaches is also possible.[18,19]

The focus of this paper is to explore the last possibility. We study the electronic structure of ternary oxides formed by the precursors TiO_2 and SnO, PbO, or Bi_2O_3. Soft x-ray spectroscopy measurements and electronic-structure calculations of TiO_2, SnO, PbO, Bi_2O_3 and ternary Sn_2TiO_4, $PbTiO_3$, $Bi_4Ti_3O_{12}$, and $Bi_2Ti_4O_{11}$ are presented, and the driving factors behind the reduction in band gap of the ternary oxides from that of pure TiO_2 are examined.

II. SYNTHESIS, MEASUREMENT, AND CALCULATION DETAILS

Synthesis. Single crystals of Sn_2TiO_4 were prepared by heating a mixture of K_2CO_3 and TiO_2 with a molar ratio of 1:1 in air at 600°–700 °C for 6 h. The product was then mixed with $SnCl_2$ with a molar ratio of Sn/Ti = 1–2. This mixture was then put into a quartz tube and dehydrated at 200 °C for 1 h in vacuum. The tube was then sealed and heated at 700 °C for 24 h. The product was washed with distilled water to remove chlorides and dried at 50 °C. The full details of the preparation and structural characterization of this material are published elsewhere.[20]

The $Bi_4Ti_3O_{12}$ powder sample was prepared from a stoichiometric mixture of Bi_2O_3 (Alfa Aesar, 99.9999%) and TiO_2 (Alfa Aesar, 99.99%) by annealing in air at 850 °C for 50 h with two intermediate grindings. The phase purity was checked with x-ray diffraction (XRD), and our results were the same as those available in the literature.[21] $PbTiO_3$ and $Bi_2Ti_4O_{11}$ were both commercially available powders (Alfa Aesar, 99.9%). Rutile TiO_2, SnO, litharge PbO, and Bi_2O_3 powders were also commercially available (Alfa Aesar, 99.9%).

Spectroscopy measurements. The x-ray emission spectroscopy (XES) measurements were performed at Beamline 8.0.1 of the Advanced light Source (ALS) at Lawrence Berkeley National Laboratory. The end station uses a Rowland circle geometry x-ray spectrometer with spherical gratings and an area sensitive multichannel detector.[22] The O K XES were excited near the O 1s ionization threshold (~540 eV) to suppress the high-energy satellite structure.[23] The spectrometer resolving power ($E/\Delta E$) for emission measurements was about 10^3.

The x-ray absorption spectroscopy (XAS) measurements were performed at the Spherical Grating Monochromator (SGM) beamline of the Canadian Light Source (CLS) at the University of Saskatchewan. The absorption measurements were acquired in total fluorescence mode (TFY) using a channel plate fluorescence detector.[24] The monochromator resolving power ($E/\Delta E$) for absorption measurements was 2×10^3. All absorption spectra were normalized to the incident photon current using a highly transparent gold mesh in front of the sample to correct for intensity fluctuations in the incident photon beam. For all x-ray measurements, the above samples were pressed into clean indium foil and measured in ultrahigh vacuum (~10^{-7}–10^{-8} Torr).

Electronic-structure calculations. Density functional theory (DFT) calculations for the experimentally determined crystal structures of ternary oxides Sn_2TiO_4 (space group $P4_2/mbc$),[20] $PbTiO_3$ (space group $P4mm$),[25] $Bi_4Ti_3O_{12}$ (space group $B2cb$),[26] $Bi_2Ti_4O_{11}$ (α phase, space group $C2/c$),[27] TiO_2 (rutile, space group $P4_2/mnm$),[28] SnO (space group $P4/nmm$),[29] PbO (litharge, space group P/nmm),[30] and Bi_2O_3 (α phase, space group $P2_1/c$) (Ref. 31) based on the full-potential augmented plane-wave method with scalar-relativistic corrections were performed using the WIEN2K code.[32] For the exchange-correlational functional, the Perdew-Burke-Ernzerhof (PBE) variant of the generalized gradient approximation[33] was used. To improve the calculated band gaps, we have also added a calculation cycle to the PBE calculation using the modified Becke Johnson (mBJ) exchange potential.[34] The atomic sphere radii (used to determine whether plane waves or spherical harmonics will be used in the expansion of the wave function) for all cases were chosen such that they were nearly touching, and $R_{MT}^{\min} K_{\max} = 7$ (the product of the smallest of the atomic sphere radii R_{MT} and the plane-wave cutoff parameter $K_{\max}$) was used for the expansion of the basis set. The Brillouin zone integrations were performed on a k-point grid of up to 1000 points (the exact number of k points depends on the symmetry of the unit cell). In all cases, the energy convergence was better than 10^{-4} Ry/unit cell and the charge convergence was better than 10^{-3} e/unit cell.

The oxygen k XES and 1s XAS were calculated from the ground-state band structure using the "XSPEC" package included with WIEN2K, which simulates the measured spectra by multiplying the partial density of states with a dipole transition matrix and a radial transition probability.[35] The calculated XES and XAS were broadened with a Lorentzian function (with an energy-dependent width varying quadratically from 0.1 eV at the upper band edge to 0.5 eV at the lower band edge) to mimic the core-hole lifetime broadening, and a Gaussian function (with an energy-dependent width based on the aforementioned experimental resolving power) to mimic the instrumental resolution.

The energy scale of the calculated XES spectra was shifted so the main spectral peak was aligned with the main spectral peak in the measured XES spectra. The calculated XAS spectra were shifted by the same amount; in this manner, the energy of the most intense measured and calculated XES spectral feature coincides for each material by design, any agreement between other calculated and measured XES or XAS features may be regarded as an indication of the accuracy of the calculation.

III. RESULTS AND DISCUSSION

The crystal structure of the ternary oxides Sn_2TiO_4, $PbTiO_3$, $Bi_4Ti_3O_{12}$, and $Bi_2Ti_4O_{11}$, in particular the local symmetry of the constituent atoms, bears some similarity to their precursor binary oxides. As shown in Fig. 1, we may separate the ternary

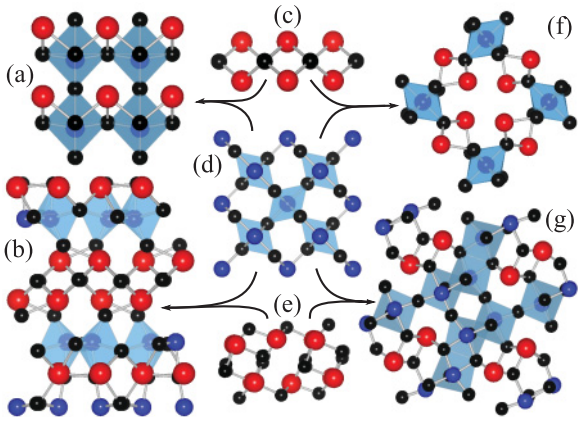

FIG. 1. (Color online) Crystal structures of the oxides studied herein. (a) $PbTiO_3$, (b) $Bi_4Ti_3O_{12}$, (c) SnO or PbO, (d) TiO_2, (e) Bi_2O_3, (f) Sn_2TiO_4, (g) $Bi_2Ti_4O_{11}$. In the case of $Bi_4Ti_3O_{12}$, only half of the unit cell is shown; the full unit cell is formed by mirroring the shown atoms upward in the plane of the page. In the other cases, slightly more than a single unit cell is shown to emphasize the site symmetry of the cations. These crystal structure diagrams were produced using VESTA 2.1.0 (Ref. 36).

oxides into two groups: those consisting of alternating layers of TiO_6 octahedra and cation-oxygen planes (namely, $PbTiO_3$ and $Bi_4Ti_3O_{12}$), and those consisting of groups of TiO_6 octahedra separated by cation-oxygen channels (namely, Sn_2TiO_4 and $Bi_2Ti_4O_{11}$).

To what degree does the similarity in local structure between the ternary oxides and their precursor binary oxides indicate a similarity in electronic structure? For an arbitrary material, we may not expect any general similarity, but for these ternary oxides there are two key factors to keep in mind:

(1) We expect the conduction band to be dominated by Ti $3d$ states (since in all cases the Ti is nominally in a $3d^0$ state), and

(2) we expect the lone-pair Sn $5s$, Pb/Bi $6s$ states to strongly affect the valence band.

In regard to the former point, the distribution of transition-metal $3d$ states is strongly driven by the local symmetry,[37,38] and since in all cases the Ti atoms are in distorted octahedra, we may expect the distribution of these states in all ternary oxides considered herein to be similar to those of the precursor TiO_2. With regard to the latter point, because the lone-pair Sn $5s$, Pb/Bi $6s$ states are nominally directed away from the ligands, and all stereochemical activity is confined to the same species of ligand, we may expect some similarity in the distribution of these states in the ternary oxides compared to the precursor binary oxides.

To examine these qualitative predictions in more detail, we turn to our x-ray spectroscopy measurements and DFT calculations of the materials in question. XES measurements involve the transitions from occupied electron states to core levels, while XAS measurements involve the transitions from core levels to unoccupied states. This process is dominated by dipole selection rules, and XES measurements involving a core level with angular momentum ℓ therefore probe the local $\ell \pm 1$ projected character of the valence band, and XAS measurements probe the local $\ell \pm 1$ projected character of the conduction band. Note that the conduction band probed by XAS is distorted from the true ground-state conduction band by the presence of a local core hole in the final state of the absorption process.

Oxygen k XES measurements (probing the $2p \rightarrow 1s$ transition) provide a good experimental probe of the ground-state oxygen $2p$ valence band. The oxygen states strongly hybridize with bonding cation states,[39–41] and consequently these measurements can provide insight into the cation electronic structure. Further, although the presence of an O $1s$ core hole in oxygen $1s$ XAS measurements (probing the $1s \rightarrow 2p$ transition) distorts the shape of the local conduction band, when oxygen is bonded to heavy cations, the core hole does not usually shift the measured XAS in energy relative to the ground-state conduction band.[41] Therefore, the combination of O k XES and $1s$ XAS can provide an estimation of the band gap (be it direct or indirect).

Electronic structure. The calculated density of states (DOS) for the ternary oxides and their precursors is shown in Fig. 2. It is immediately clear that the electronic structures of these materials have many aspects in common. As we expect, the valence band in all of these materials is dominated by O $2p$ states. Where Ti $3d$ states are present, they are hybridized with the O $2p$ states, primarily at 4–5 eV below

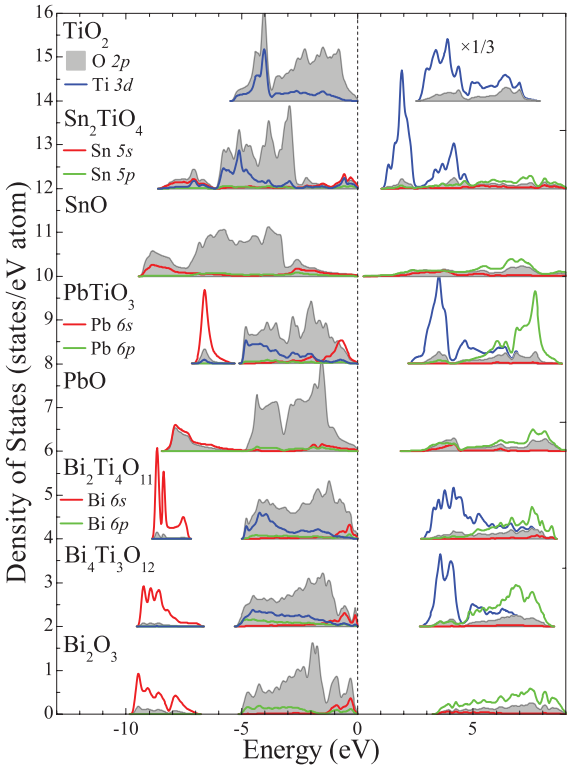

FIG. 2. (Color online) Calculated DOS of the materials studied herein. The top of the valence band is at 0 eV. (For brevity, we will call the top of the valence band the "Fermi level," even though technically the Fermi level is undefined for band-gap materials.) The calculations predict that all materials have a band gap, although the gap for SnO is quite small. The conduction-band Ti $3d$ states have been reduced in amplitude by a factor of 3. Note how the lone-pair cation states (Sn $5s$, Pb, and Bi $6s$) are split into bonding and antibonding states at the bottom and top of the valence band, respectively.

the Fermi level. These Ti $3d$ states dominate the onset of the conduction band as well, and typically are separated into two different features (although the separation is weak for $Bi_2Ti_4O_{11}$); a rather sharp feature directly at the onset of the conduction band, and a somewhat less intense feature at 2–3 eV higher in the conduction band. Since the Ti sites are almost octahedral, the low- and high-energy Ti $3d$–O $2p$ conduction-band hybridization regions are often referred to as e_g and t_{2g} bands, respectively.[42,43] The heavy cation p states (Sn $5p$, Pb, and Bi $6p$) have an almost negligible contribution to the valence band, and only make a significant contribution to the conduction band at about 5 eV above the Fermi level.

The lone-pair cation states (Sn $5s$, Pb, and Bi $6s$) provide a significant contribution to the valence band. These states are also hybridized with O $2p$ states, and bonding between O and the heavy cation create a O $2p$ cation ns band at the bottom of the valence band. This band is actually separate from the main valence band for materials with Bi and, to a lesser extent, Pb. There is also a weaker, but still significant, O $2p$ cation ns antibonding region at the Fermi level. This lone-pair hybridization is consistent with previous studies.[44–46] It is worth noting that one can qualitatively see the effects of combining the lone-pair oxides with TiO_6 octahedra in the DOS of the ternary oxides. In all cases, the bonding O $2p$ cation

ns states of the ternary oxides are shifted to slightly higher energies than the corresponding states in the binary oxides. Similarly, the Ti 3*d* states at the onset of the conduction band are shifted toward the onset of the conduction band in the lone-pair oxide. This is easiest to see in the case of Sn_2TiO_4: SnO is calculated to have a very narrow band gap, and the conduction Ti 3*d* states in Sn_2TiO_4 are about 2 eV lower in energy than the corresponding states in TiO_2. This trend also occurs in $PbTiO_3$, $Bi_2Ti_4O_{11}$, and $Bi_4Ti_3O_{12}$, although it is harder to see (the Ti 3*d* conduction states in $PbTiO_3$ start ∼0.4 eV lower in energy than in TiO_2, while the corresponding states in $Bi_2Ti_4O_{11}$ and $Bi_4Ti_3O_{12}$ are ∼0.2 eV higher in energy). Finally, in the case of $PbTiO_3$ and Sn_2TiO_4, the antibonding cation *ns* states at the Fermi level are more localized in energy; this is probably due to the greater concentration of states at the Fermi level in the TiO_6 octahedra (relative to pure SnO and PbO) limiting the curvature of the band structure. These observations suggest there is some merit to our initial hypothesis that the electronic structure of a d^0 lone-pair ternary oxide may be described in terms of the electronic structure of both binary precursors.

X-ray spectroscopy. The measured and calculated O *k* XES and 1*s* XAS spectra are shown in Fig. 3. The calculated O *k* XES spectra generally agree quite well with the measured ones. There is also reasonable agreement between the calculated and measured O 1*s* XAS spectra, although since our calculations did not include a core hole, we do not expect the agreement

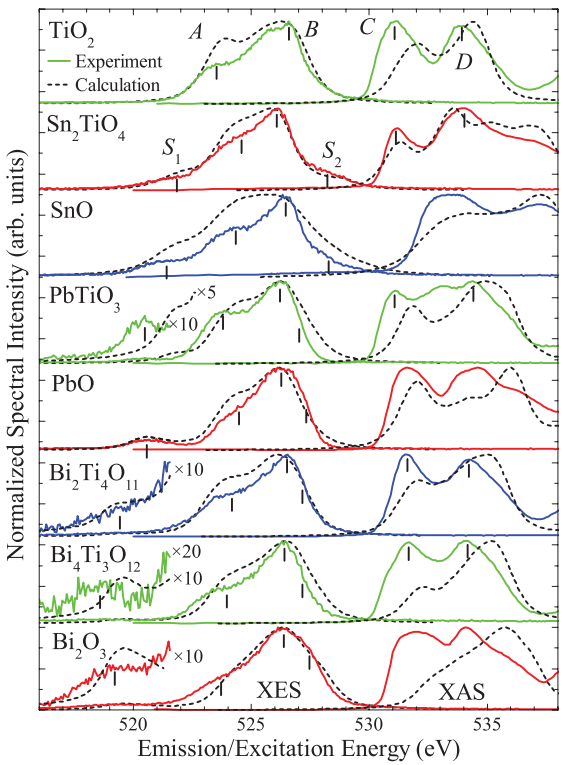

FIG. 3. (Color online) Measured and calculated O *k* XES and 1*s* XAS spectra of the materials studied herein. The calculated spectra were shifted so the main O *K* XES peak was aligned with the experimental peak. The key spectral features (labeled S_1, *A*, *B*, S_2, *C*, and *D*) are denoted by small black lines on each spectrum. Note TiO_2 lacks the $S_{1,2}$ XES features, while SnO, PbO, and Bi_2O_3 lack the *C*, *D* XAS features.

to be perfect. In fact, since the XES measurements agree with the calculations, we can attribute the differences between the measured and calculated XAS spectra to the influence of the O 1s core hole. We have previously found that the main influence of an O 1*s* core hole is to increase the intensity of the XAS at the bottom of the conduction band;[41] this seems to be true for the ternary and binary oxides studied herein as well, although the O 1*s* core hole seems to shift the XAS to lower energies in Bi_2O_3 (by about 1 eV), and to a lesser extent, in $Bi_4Ti_3O_{12}$ (by about 0.5 eV). In contrast, the O 1s core hole seems to have a minor effect on the XAS of Sn_2TiO_4 and SnO.

The measured spectra have several features in common. The TiO_2 XES spectrum shows two clear features (labeled *A* and *B* in Fig. 3), which we can attribute to O 2*p*–Ti 3*d* hybridization for *A*, and O 2*p* states for *B* with the help of the DOS calculations shown in Fig. 2. The TiO_2 XAS spectrum also has two clear near-edge features, labeled *C* and *D*, and these can be attributed to O 2*p* hybridization with the Ti 3*d* e_g and t_{2g} bands. The ternary and binary oxides containing lone pairs also show low-energy structure in their XES spectrum that is related to bonding O 2*p*–cation *ns* states, labeled S_1 in Fig. 3. There is also high-energy structure in the O XES spectrum of SnO, Sn_2TiO_4, PbO, and Bi_2O_3 that is related to antibonding O 2*p*–cation *ns* states (labeled S_2). This identification of the S_1 and S_2 features follows from analysis of the calculated DOS discussed previously. Identifying S_2 in the XES spectrum of $PbTiO_3$, $Bi_2Ti_4O_{11}$, and $Bi_4Ti_3O_{12}$ is difficult, and not unambiguous. However, since the calculated XES spectra for these materials do not suggest any discontinuous behavior from the main O 2*p* states at *B* to the Fermi level, this is not unexpected. Small vertical bars in Fig. 3 denote the features S_1, *A*, *B*, S_2, *C*, and *D* in the XES and XAS for each compound. Note that in the binary oxides SnO, PbO, and Bi_2O_3, we attribute feature *B* to O 2*p*–cation *np* hybridization, as suggested by the DOS in Fig. 2.

There are two general observations one may make about the measured compared to the calculated XES spectra: The main peak *B* is typically sharper and more intense relative to the other spectral features in the measured spectrum than predicted by the calculated spectrum. This is likely due to lattice defects in the materials destroying the perfect crystalline periodicity assumed by the calculations, and consequently introducing a greater localization of states. The other general observation is that, save for PbO and perhaps SnO, the S_1 spectral feature is at lower energies than predicted by the calculated spectrum. This may be due to the calculation underestimating O 2*p*–cation *np* bonding affinity. We also note that S_1 in the ternary oxides Sn_2TiO_4 and $PbTiO_3$ is closer in energy to S_1 in their parent binary oxides (SnO and PbO, respectively) than suggested by the calculation; this indicates that the calculation may overestimate the influence of TiO_6 octahedra on the bonding structure. Despite these differences, however, the basic agreement in features, relative intensities, and energy spacings of the calculated and measured XES and XAS spectra suggest that our calculated DOS is accurate for these systems.

O 2p hybridization with cations. We can use our experimental XES spectra to quantitatively estimate the strength of the O 2*p*–cation *ns* bonding by taking the ratio of the integrated intensity of the S_1 XES feature I_{S_1} to the integrated intensity of the total XES spectrum I_{tot}, and dividing by the ratio of the

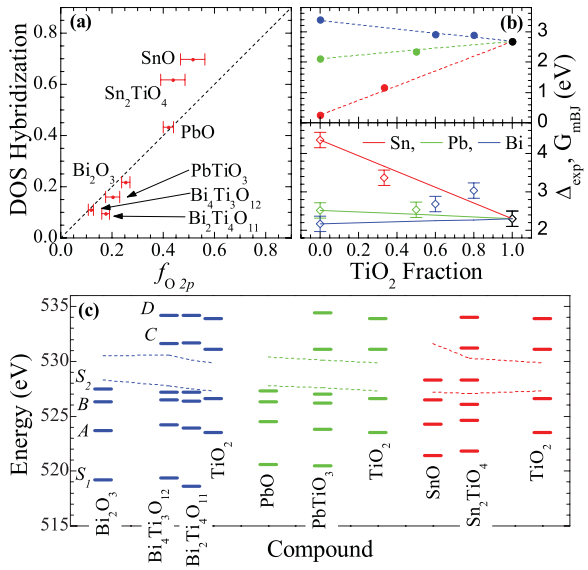

FIG. 4. (Color online) (a) $f_{O\,2p}$ derived from the XES compare to the calculated DOS hybridization [O $2p$/(O$2p$ + cationns) using the calculated DOS]. The error bars denote the approximate spread of $f_{O\,2p}$ if the estimated end of region S_1 is shifted by ±0.2 eV, the straight line indicates perfect agreement between $f_{O\,2p}$ and the DOS hybridization. (b) The calculated band gaps (G_{mBJ}, top) and estimated spectral gaps (Δ_{exp}, bottom) for these materials, expressed as a fraction of the TiO_2 content. The lines indicate a linear change in gap with TiO_2 content. (c) The energy of the measured XES spectral features as a function of TiO_2 content the lines of the Fermi level and the bottom of the conduction band estimated using the second derivative maxima.

number of cation atoms n and the number of electron pairs p per formula unit of the lone-pair binary oxide. This analysis for Bi_2O_3 and PbO is available in the literature,[45] and is commonly called the $f_{O\,2p}$ value:

$$f_{O\,2p} = \frac{I_{S_1}}{I_{tot}}\left(\frac{p}{n}\right).$$

Our estimates for $f_{O\,2p}$ are shown in Fig. 4(a). These empirical values can be compared directly to the ratio of the total O $2p$ states to the total O $2p$ and cation ns states in this region (using the calculated DOS).[45]

The technique of using $f_{O\,2p}$ to estimate the degree of O $2p$–cation ns hybridization is justified, given the agreement shown in Fig. 4(a). Importantly, we can also estimate whether $f_{O\,2p}$ will overestimate or underestimate the hybridization by a qualitative inspection of the XES. Referring back to Fig. 3, we see that in the case of SnO and Sn_2TiO_4, the S_1 feature is relatively intense and is more of a shoulder to the main XES emission than a separate feature. We can therefore predict that $f_{O\,2p}$ will be an underestimate of the true hybridization since the S_1 feature probably extends somewhat into the main XES. On the other hand, for Bi_2O_3 and $Bi_2Ti_4O_{11}$, the S_1 feature is relatively quite weak. We can therefore predict that $f_{O\,2p}$ will be an overestimate of the true hybridization since the broadened emission from the main DOS region will extend into S_1, providing a significant contribution to the weak hybridization emission. $Bi_4Ti_3O_{12}$ has lowest intensity S_1 feature, but this feature is also quite low in energy. The separation of this feature from the emission band minimizes the amount of "leakage" that can occur through broadening. We therefore expect that $f_{O\,2p}$ will be quite close to the true DOS hybridization, as indeed it is.

Indeed, the impact of spectral broadening on $f_{O\,2p}$ is evident in $Bi_4Ti_3O_{12}$: the calculated XES has roughly double the S_1 intensity as the measured XES (refer back to Fig. 3), although $f_{O\,2p}$ is in excellent agreement with the DOS hybridization [refer to Fig. 4(a)]. Note that S_1 in the calculated XES is also about 1.5 higher in energy; it is therefore likely that the broadening of the main A and B features into S_1 is responsible for the larger intensity (this also probably applies to $PbTiO_3$, where a similar situation occurs). Finally, we should mention that the broadening applied to the calculated spectra was merely a "best guess"; it could easily have been somewhat too large.

Band-gap estimates. In our previous research on binary and ternary oxides, we have shown that the separation between the local maxima in the second derivatives of the O k XES and 1s XAS spectra provides a reasonably consistent method for estimating the band gap.[41,47,48] This is not a particularly rigorous method of determining the band edges, indeed it is only correct for DOS which exhibit a limited range of behaviors near the band edge (here "near" means within the effective range of the spectral broadening), such as being linear or parabolic in energy. Looking back at Fig. 2, we may anticipate that the second derivative method will provide reasonable estimates of the band gap for TiO_2 and the Bi-based compounds since they all have relatively sharp and smooth behavior near the Fermi level and the bottom of the conduction band. In the Sn-based materials, however, the valence band and (and conduction band for SnO) have very gradual onsets, and it is unlikely that a single second derivative maximum can be unambiguously determined at the band edges. Note also that even if the DOS is shaped appropriately for the second derivative method, the aforementioned core-hole shift will cause the x-ray "spectral gap" to be less than the true ground-state band gap.

With these caveats in mind, it is worthwhile mentioning the estimated gap (Δ_{exp}) for these materials to compare with the calculated band gap (G_{mBJ}) and values obtained from previous studies. These values are shown in Table I. As we expected, the

TABLE I. Measured, calculated, and previously reported band gaps for all materials studied herein. The measured gaps are denoted by Δ_{exp} and the calculated band gaps are denoted by G_{mBJ}. The literature band gaps are all based on optical measurements save for Sn_2TiO_4, which is exclusively based on a calculation. The second value for SnO is the estimated indirect gap from the measurement of 2.7 eV for the direct gap.

Compound	Δ_{exp} (±0.2 eV)	G_{mBJ} (eV)	Literature (eV)
TiO_2	2.6	2.679	3.03 (Ref. 3)
Sn_2TiO_4	3.4	1.170	2.09 (Ref. 49)
SnO	4.2	0.254	2.7, ∼0.7 (Ref. 50)
$PbTiO_3$	2.6	2.336	3.4 (Ref. 51)
PbO	2.5	2.116	2.75 (Ref. 52)
$Bi_2Ti_4O_{11}$	2.8	2.887	3.75 (Ref. 53)
$Bi_4Ti_3O_{12}$	2.4	2.919	3.08 (Ref. 54)
Bi_2O_3	2.2	3.388	2.91 (Ref. 55)

Δ_{exp} spectral gap for SnO is considerably larger than both our calculated gap and those obtained from optical measurements; because of the extremely gradual onset of both the valence and the conduction bands, we expect this value to be an overestimate. Indeed, the second derivative maximum of the SnO O k XES is at 527.2 eV, which is above the S_2 antibonding feature, and therefore clearly not at the Fermi level. In the same sense, the Fermi level of Sn_2TiO_4 is also not accurately estimated by the XES second derivative maximum (this is at 526.9 eV, again above S_2), although the XAS second derivative maximum is within 0.1 eV of the calculated conduction-band onset. For TiO_2, PbO, $PbTiO_3$, and $Bi_2Ti_4O_{11}$, the spectral gaps Δ_{exp} are quite similar to the calculated gaps. If we add the estimated core-hole shifts for Bi_2O_3 and $Bi_4Ti_3O_{12}$ mentioned above to Δ_{exp}, then we again get good agreement, but since the core-hole shifts here were estimated by comparing the calculated and measured XAS, the agreement is admittedly a bit contrived.

The band gaps reported from the literature in Table I are all derived from optical measurements, most of which were only probing the direct band gap. For SnO, the indirect gap was estimated as ~0.7 eV from the optical data, but this analysis is not available for the other lone-pair oxides Bi_2O_3 and PbO. Calculated band structures suggest these are all indirect band-gap materials, so we may expect the literature values for PbO and Bi_2O_3 in Table I to overestimate the gap. For Bi_2O_3, this perhaps suggests that our larger calculated gap may be a rare overestimate of a band gap by DFT (it is well known that DFT underestimates band gaps[56]).

Trends in electronic structure: Due to the previously discussed features in the electronic structure particular to these binary and ternary oxides, namely, the lone-pair ns states bounding the valence band and the Ti 3d states defining the bottom of the conduction band, if we treat the ternary oxides as a mixture of the two precursor binary oxides, i.e., Sn_2TiO_4 is treated as $(SnO)_{2/3}(TiO_2)_{1/3}$, the calculated band gaps show an almost linear dependence on the mixing fraction, as shown in Fig. 4(b). Interestingly, the estimated spectral gaps Δ_{exp} for the Sn- and Pb-based compounds also show an almost linear dependence, despite the aforementioned inaccuracy of Δ_{exp} as an estimate of the band gap for SnO and Sn_2TiO_4. There is no linear trend in Δ_{exp} for the Bi-based compounds, but this is perhaps due to the anomalous core-hole effect on Bi_2O_3, as discussed above ("anomalous" in the fact that it appears to disproportionally affect Bi_2O_3 over any of the other Bi-based compounds).

Further, while Δ_{exp} does not necessarily indicate the band gap of a compound with lone-pair s states, it can be used to determine whether a ternary oxide abides by this rule. If the Δ_{exp} of the ternary compound obtained from O k XES and 1s XAS is close to the "ideal" value (again by stoichiometry-weighted addition of Δ_{exp} of the parent oxides), then the band gap of the ternary compound may be inferred to be the stoichiometry-weighted addition of the band gaps of the parent oxides. This is useful because ternary oxides with a dilute stoichiometric addition of a particular parent oxide may have complicated crystal structures and make calculating their properties directly a computationally intensive task.

This is demonstrated by the energies of the XES spectral features, shown in Fig. 3 and summarized in Fig. 4(c). In Fig. 4(c), we see how the TiO_2 content gradually lowers the energy of the antibonding S_2 feature at the top of the valence band [note that the dotted lines in Fig. 4(c) show the band edges estimated using the second derivative maxima, and here the problem with using the method for SnO and Sn_2TiO_4 is clear since S_2 is at higher energies than the second derivative maxima]. Conversely, the presence of TiO_2 seems to stabilize the conduction band (features C and D).

This simple agreement in both calculated and measured data suggests that the true band gap of a ternary oxide formed from lone pair and a d^0 binary oxide is directly related to the stoichiometry-weighted addition of the band gaps of the precursors: in the examples studied herein, the conduction band is qualitatively defined by the Ti 3d^0 states, but increasing the stoichiometric content of lone pair oxides is responsible for progressively "dragging" of the conduction-band edge to energies closer to that of the pure lone-pair oxide. The same argument applies to the valence-band edge; while it is qualitatively defined by antibonding s^2 states, increasing stoichiometric content of TiO_2 can "drag" the valence-band edge closer to that of pure TiO_2.

Conclusions. To summarize, we have probed the electronic structure of ternary oxides Sn_2TiO_4, $PbTiO_3$, $Bi_4Ti_3O_{12}$, and $Bi_2Ti_4O_{11}$ using O k XES, 1s XAS, and DFT calculations. These ternary oxides are formed from precursor binary lone-pair oxides (SnO, PbO, and Bi_2O_3) and the d^0 oxide TiO_2. We find that key features in the electronic structure of the precursor oxides, such as the valence band being bounded by bonding and antibonding Sn 5s, Pb 6s, or Bi 6s states hybridized with O 2p states in SnO, PbO, and Bi_2O_3, and the conduction band being primarily defined by Ti 3d states in TiO_2, are preserved in the ternary oxides. Importantly, we find that the band gap of a ternary oxide with a TiO_2 fraction of x basically falls on the straight line between that of TiO_2 ($x = 1$) and the lone-pair parent oxide ($x = 0$). A similar trend in the gap between the peaks in the second derivative of the O k XES and 1s XAS of these oxides suggests that this trend is a property of the general electronic structure, and that O k XES and 1s XAS spectroscopy can be an experimental way of testing the idea that the band gap of a lone pair, d^0 ternary oxide is the stoichiometry-weighted addition of the band gaps of the parent lone pair and d^0 binary oxides. These findings can be used to predict the band gap of new ternary oxides if the band gaps of the parent lone pair and d^0 binary oxides are known.

ACKNOWLEDGMENTS

We acknowledge support of the Natural Sciences and Engineering Research Council of Canada (NSERC), the Canada Research Chair program, and the Russian Foundation for Basic Research (Projects 11-02-00022). The Canadian Light Source is supported by the NSERC, the National Research Council (NSC) Canada, the Canadian Institutes of Health Research (CIHR), the Province of Saskatchewan, Western Economic Diversification Canada, and the University of Saskatchewan. The Advanced Light Source is supported by the Director, Office of Science, Office of Basic Energy Sciences, of the US Department of Energy under Contract No. DE-AC02-05CH11231.

*john.mcleod@usask.ca

[1] R. Asahi, T. Morikawa, T. Ohwaki, K. Aoki, and Y. Taga, Science **293**, 269 (2001).

[2] A. Fujishima and K. Honda, Nature (London) **238**, 37 (1972).

[3] J. Pascual, J. Camassel, and H. Mathieu, Phys. Rev. Lett. **39**, 1490 (1977).

[4] H. Tang, H. Berger, P. E. Schmid, and F. Lévy, Solid State Commun. **92**, 267 (1994).

[5] R. Sharma, P. P. Das, M. Misra, V. Mahajan, J. P. Bock, S. Trigwell, A. S. Biris, and M. K. Mazumder, Nanotechnology **20**, 075704 (2009).

[6] D. Y. C. Leung, X. Fu, C. Wang, M. Ni, M. K. H. Leung, X. Wang, and X. Fu, ChemSusChem **3**, 681 (2010).

[7] H. Irie, Y. Watanabe, and K. Hashimoto, J. Phys. Chem. B **107**, 5483 (2003).

[8] S. Khan, M. Al-Shahry, and W. B. Ingler Jr., Science **297**, 2243 (2002).

[9] S.-C. Moon, H. Mametsuka, S. Tabata, and E. Suzuki, Catal. Today **58**, 125 (2000).

[10] T.-H. Xu, C.-L. Song, Y. Liu, and G.-R. Han, J. Zhejiang Univ. Sci. B **7**, 299 (2006).

[11] N. Serpone, J. Phys. Chem. B **110**, 24287 (2006).

[12] L. Tsetseris, Phys. Rev. B **81**, 165205 (2010).

[13] T. Umebayashi, T. Yamaki, H. Itoh, and K. Asai, J. Phys. Chem. Solids **63**, 1909 (2002).

[14] Y. Yang, X.-J. Li, J.-T. Chen, and L.-Y. Wang, J. Photochem. Photobiol. A **163**, 517 (2004).

[15] A. Schleife, F. Fuchs, J. Furthmüller, and F. Bechstedt, Phys. Rev. B **73**, 245212 (2006).

[16] A. Walsh, SPIE Newsroom (2009), doi:10.1117/2.1200905.1608.

[17] J. Moon, H. Takagi, Y. Fujishiro, and M. Awano, J. Mater. Sci. **36**, 949 (2001).

[18] W.-J. Yin, H. Tang, S.-H. Wei, M. M. Al-Jassim, J. Turner, and Y. Yan, Phys. Rev. B **82**, 045106 (2010).

[19] P. Wang, Z. Liu, F. Lin, G. Zhou, J. Wu, W. Duan, B.-L. Gu, and S. B. Zhang, Phys. Rev. B **82**, 193103 (2010).

[20] N. Kumada, Y. Yonesaki, T. Takei, N. Kinomura, and S. Wada, Mater. Res. Bull. **44**, 1298 (2009).

[21] Y. Noguchi, T. Goto, M. Miyamama, A. Hoshikawa, and T. Kamiyama, J. Electroceram. **21**, 49 (2008).

[22] J. J. Jia, T. A. Callcott, J. Yurkas, A. W. Ellis, and F. J. Himpsel, Rev. Sci. Instrum. **66**, 1394 (1995).

[23] J. Valjakka, J. Utriainen, T. Åberg, and J. Tulkki, Phys. Rev. B **32**, 6892 (1985).

[24] T. Regier, J. Krochak, T. K. Sham, Y. F. Hu, J. Thompson, and R. I. R. Blyth, Nulc. Instrum. Meth. A **582**, 93 (2007).

[25] A. M. Glazer and S. A. Mabud, Acta Crystallogr. Sect. B **34**, 1065 (1978).

[26] While $Bi_4Ti_3O_{12}$ was recently reported to have $B2cb$ symmetry (Ref. 57), there are a few earlier reports that $Bi_4Ti_3O_{12}$ is best represented by the $B1a1$ space group at ambient conditions (Refs. 58 and 59). Since other studies have noted that there is very little difference between the two structures (Refs. 60 and 61), and *ab initio* calculations reveal little difference in the energy stability (Ref. 62) between the two phases, we feel justified in using the $B2cb$ phase herein. Indeed, there is little difference in the bulk electronic structure of the $B1a1$ phase and the higher-symmetry $I4/mmm$ phase (realized above 700 °C) (Ref. 21).

[27] V. Kahlenberg and H. Böhm, Acta Crystallogr. Sect. B **51**, 11 (1995).

[28] R. J. Swope, J. R. Smyth, and A. C. Larson, Am. Mineral. **80**, 448 (1995).

[29] X. Wang, F. X. Zhang, I. Loa, K. Syassen, M. Hanfland, and Y.-L. Mathis, Phys. Status Solidi B **241**, 3168 (2004).

[30] P. Boher, P. Garnier, J. R. Gavarri, and A. W. Hewat, J. Solid State Chem. **57**, 343 (1985).

[31] G. Malmros, Acta Chem. Scand. **24**, 384 (1970).

[32] P. Blaha, K. Schwarz, G. K. H. Madsen, D. Kvasnicka, and J. Luitz, *WIEN2k, An Augmented Plane Wave + Local Orbitals Program for Calculating Crystal Properties* (Karlheinz Schwarz, Techn. Universität Wien, Austria, 2001).

[33] J. P. Perdew, K. Burke, and M. Ernzerhof, Phys. Rev. Lett. **77**, 3865 (1996).

[34] F. Tran and P. Blaha, Phys. Rev. Lett. **102**, 226401 (2009).

[35] K. Schwarz, A. Neckel, and J. Nordgren, J. Phys. F: Met. Phys. **9**, 2509 (1979).

[36] K. Momma and F. Izumi, J. Appl. Crystallogr. **41**, 653 (2008).

[37] J. D. Dunitz and L. E. Orgel, J. Phys. Chem. Solids **3**, 20 (1957).

[38] G. W. Ludwig and H. H. Woodbury, Phys. Rev. Lett. **5**, 98 (1960).

[39] A. Walsh and G. W. Watson, Phys. Rev. B **70**, 235114 (2004).

[40] M. W. Stoltzfus, P. W. Woodward, R. Seshadri, J.-H. Klepeis, and B. Bursten, Inorg. Chem. **46**, 3839 (2007).

[41] J. A. McLeod, R. G. Wilks, N. A. Skorikov, L. D. Finkelstein, M. Abu-Samak, E. Z. Kurmaev, and A. Moewes, Phys. Rev. B **81**, 245123 (2010).

[42] F. M. F. de Groot, M. Grioni, J. C. Fuggle, J. Ghijsen, G. A. Sawatzky, and H. Petersen, Phys. Rev. B **40**, 5715 (1989).

[43] F. M. F. de Groot, J. Faber, J. J. M. Michiels, M. T. Czyžyk, M. Abbate, and J. C. Fuggle, Phys. Rev. B **48**, 2074 (1993).

[44] A. Walsh, D. J. Payne, R. G. Egdell, and G. W. Watson, Chem. Soc. Rev. **40**, 4455 (2011).

[45] A. Walsh, G. W. Watson, D. J. Payne, R. G. Edgell, J. Guo, P.-A. Glans, T. Learmonth, and K. E. Smith, Phys. Rev. B **73**, 235104 (2006).

[46] U. V. Waghmare, N. A. Spaldin, H. C. Kandpal, and R. Seshadri, Phys. Rev. B **67**, 125111 (2003).

[47] J. A. McLeod, Z. V. Pchelkina, L. D. Finkelstein, E. Z. Kurmaev, R. G. Wilks, A. Moewes, I. V. Solovyev, A. A. Belik, and E. Takayama-Muromachi, Phys. Rev. B **81**, 144103 (2010).

[48] E. Z. Kurmaev, R. G. Wilks, A. Moewes, L. D. Finkelstein, S. N. Shamin, and J. Kunes, Phys. Rev. B **77**, 165127 (2008).

[49] C. R. A. Catlow, Z. X. Guo, M. Miskufova, S. A. Shevlin, A. G. H. Smith, A. A. Sokol, A. Walsh, D. J. Wilson, and S. M. Woodley, Philos. Trans. R. Soc., A **368**, 3379 (2010).

[50] Y. Ogo, H. Hiramatsu, K. Nomura, H. Yanagi, T. Kamiya, M. Hirano, and H. Hosono, Appl. Phys. Lett. **93**, 032113 (2008).

[51] W. L. Warren, J. Robertson, D. Dimos, B. A. Tuttle, G. E. Pike, and D. A. Payne, Phys. Rev. B **53**, 3080 (1996).

[52] R. C. Keezer, D. L. Bowmand, and J. H. Becker, J. Appl. Phys. **39**, 2062 (1968).

[53] T. Kidchob, L. Malfatti, D. Marongiu, S. Enzo, and P. Innocenzi, J. Am. Ceram. Soc. **93**, 2897 (2010).

[54] H. Zhang, G. Chen, and X. Li, Solid State Ionics **180**, 1599 (2009).

[55] H. Gobrecht, S. Seeck, H.-E. Bergt, A. Märtens, and K. Kossmann, Phys. Status Solidi **33**, 599 (1969).

[56] P. Dufek, P. Blaha, and K. Schwarz, Phys. Rev. B **50**, 7279 (1994).

[57]K. R. Chakraborty, S. N. Achary, S. J. Patwe, P. S. R. Krishna, A. B. Shinde, and A. K. Tyagi, Ceram. Int. **33**, 601 (2007).
[58]A. D. Rae, J. G. Thompson, R. L. Withers, and A. C. Willis, Acta Crystallogr. Sect. B: Struct. Sci. **46**, 474 (1990).
[59]Y.-I. Ki and M. K. Jeon, Mater. Lett. **58**, 1889 (2004).
[60]C. H. Hervoches and P. Lightfoot, Chem. Mater. **11**, 3359 (1999).
[61]T. Hashimoto and H. Moriwake, Phys. Rev. B **78**, 092106 (2008).
[62]A. Shrinagar, A. Garg, R. Prasad, and S. Auluck, Acta Crystallogr. Sect. A: Found. Crysyallogr. **64**, 368 (2008).